The Astrophysical Journal Letters, 933:L23 (8pp), 2022 July 1 https://doi.org/10.3847/2041-8213/ac7442

An Isolated Mass-gap Black Hole or Neutron Star Detected with Astrometric Microlensing

Casey Y. Lam[1], Jessica R. Lu[1], Andrzej Udalski[2,17], Ian Bond[3,18], David P. Bennett[4,5,18], Jan Skowron[2,17], Przemek Mróz[2,17], Radek Poleski[2,17], Takahiro Sumi[6,18], Michał K. Szymański[2,17], Szymon Kozłowski[2,17], Paweł Pietrukowicz[2,17], Igor Soszyński[2,17], Krzysztof Ulaczyk[2,7,17], Łukasz Wyrzykowski[2,17], Shota Miyazaki[6,18], Daisuke Suzuki[6,18], Naoki Koshimoto[4,5,8,18], Nicholas J. Rattenbury[9,18], Matthew W. Hosek, Jr.[10], Fumio Abe[11,18], Richard Barry[4,18], Aparna Bhattacharya[4,5,18], Akihiko Fukui[12,13,18], Hirosane Fujii[11,18], Yuki Hirao[6,18], Yoshitaka Itow[11,18], Rintaro Kirikawa[6,18], Iona Kondo[6,18], Yutaka Matsubara[11,18], Sho Matsumoto[6,18], Yasushi Muraki[11,18], Greg Olmschenk[4,18], Clément Ranc[14,18], Arisa Okamura[6], Yuki Satoh[6], Stela Ishitani Silva[4,15,18], Taiga Toda[6,18], Paul J. Tristram[16,18], Aikaterini Vandorou[4,5,18], Hibiki Yama[6,18], Natasha S. Abrams[1], Shrihan Agarwal[1], Sam Rose[1], and Sean K. Terry[1]

[1] University of California, Berkeley, Department of Astronomy, Berkeley, CA 94720, USA; casey_lam@berkeley.edu
[2] Astronomical Observatory, University of Warsaw, Al. Ujazdowskie 4,00-478 Warszawa, Poland
[3] School of Mathematical and Computational Sciences, Massey University, Private Bag 102-904 North Shore Mail Centre, Auckland 0745, New Zealand
[4] Code 667, NASA Goddard Space Flight Center, Greenbelt, MD 20771, USA
[5] Department of Astronomy, University of Maryland, College Park, MD 20742, USA
[6] Department of Earth and Space Science, Graduate School of Science, Osaka University, Toyonaka, Osaka 560-0043, Japan
[7] Department of Physics, University of Warwick, Gibbet Hill Road,Coventry, CV4 7AL, UK
[8] Department of Astronomy, Graduate School of Science, The University of Tokyo, 7-3-1 Hongo, Bunkyo-ku, Tokyo 113-0033, Japan
[9] Department of Physics, University of Auckland, Private Bag 92019, Auckland, New Zealand
[10] University of California, Los Angeles, Department of Astronomy, Los Angeles, CA 90095, USA
[11] Institute for Space-Earth Environmental Research, Nagoya University, Nagoya 464-8601, Japan
[12] Department of Earth and Planetary Science, Graduate School of Science, The University of Tokyo, 7-3-1 Hongo, Bunkyo-ku, Tokyo 113-0033, Japan
[13] Instituto de Astrofísica de Canarias, Vía Láctea s/n, E-38205 La Laguna, Tenerife, Spain
[14] Zentrum für Astronomie der Universität Heidelberg, Astronomisches Rechen-Institut, Mönchhofstr. 12–14, D-69120 Heidelberg, Germany
[15] Department of Physics, The Catholic University of America, Washington, DC 20064, USA
[16] University of Canterbury Mt. John Observatory, P.O. Box 56, Lake Tekapo 8770, New Zealand
Received 2022 February 3; revised 2022 May 19; accepted 2022 May 27; published 2022 July 6

Abstract

We present the analysis of five black hole candidates identified from gravitational microlensing surveys. Hubble Space Telescope astrometric data and densely sampled light curves from ground-based microlensing surveys are fit with a single-source, single-lens microlensing model in order to measure the mass and luminosity of each lens and determine if it is a black hole. One of the five targets (OGLE-2011-BLG-0462/MOA-2011-BLG-191 or OB110462 for short) shows a significant >1 mas coherent astrometric shift, little to no lens flux, and has an inferred lens mass of 1.6–4.4 $M_{\odot}$. This makes OB110462 the first definitive discovery of a compact object through astrometric microlensing and it is most likely either a neutron star or a low-mass black hole. This compact-object lens is relatively nearby (0.70–1.92 kpc) and has a slow transverse motion of $<30\,\mathrm{km\,s^{-1}}$. OB110462 shows significant tension between models well fit to photometry versus astrometry, making it currently difficult to distinguish between a neutron star and a black hole. Additional observations and modeling with more complex system geometries, such as binary sources, are needed to resolve the puzzling nature of this object. For the remaining four candidates, the lens masses are $<2M_{\odot}$, and they are unlikely to be black holes; two of the four are likely white dwarfs or neutron stars. We compare the full sample of five candidates to theoretical expectations on the number of black holes in the Milky Way ($\sim 10^8$) and find reasonable agreement given the small sample size.

Unified Astronomy Thesaurus concepts: Astrophysical black holes (98); Astrometric microlensing effect (2140); Stellar populations (1622); Astrometry (80)

1. Introduction

Stellar-mass black holes are produced when massive stars collapse under their own gravity. Observations of black holes (BHs) are a key ingredient for understanding outstanding questions in massive stellar evolution, such as which stars explode, which stars produce neutron stars versus BHs, and whether there is a gap between the heaviest neutron stars (NSs) and the lightest BHs.

Black holes are abundant. There are predicted to be 10^7–10^9 stellar-mass BHs in the Milky Way alone (Shapiro & Teukolsky 1983; Timmes et al. 1996; Samland 1998; Agol et al. 2002; Sartore & Treves 2010). However, only about two dozen have been definitively detected, all in binaries with dynamical mass measurements (Corral-Santana et al. 2016; Thompson et al. 2019). Beyond the Milky Way, over 80 binary BH mergers have been detected via gravitational waves, with

[17] OGLE collaboration.
[18] MOA collaboration.

component masses spanning the lower mass gap $\sim 3M_\odot$ to the lower intermediate-mass BH range $\sim 100M_\odot$ (Abbott et al. 2020).

These BHs are not a representative sample of the population, as they are all in binary systems. While most massive stars exist in binary or multiple systems (Sana 2017), the majority of the BH population is expected to be isolated due to the disruption of the progenitor systems (Belczynski et al. 2004; Fender et al. 2013; Wiktorowicz et al. 2019).

Isolated BHs in the Milky Way can be found and weighed using the technique of gravitational microlensing. When a foreground lens (e.g., BH) passes in front of a background source star, the source light is temporarily bent and split into two unresolved images by the lens mass, producing a transient photometric and astrometric signal (Paczynski 1986; Hog et al. 1995; Miyamoto & Yoshii 1995; Walker 1995). The characteristic cross section of a microlensing event is set by the angular Einstein radius, $\theta_E = \sqrt{\kappa M_L(\pi_L - \pi_S)}$, and depends on the lens mass (M_L) and the parallax of the lens (π_L) and source (π_S), where $\kappa = 4G/(1\ \mathrm{au} \cdot c^2) = 8.14\ \mathrm{mas}/M_\odot$ is a constant. A $\sim 10\ M_\odot$ BH in the Milky Way disk lensing a background bulge star typically has a $\theta_E = 1-3$ mas.

Photometric light curves can measure the duration of the event, $t_E = \theta_E/\mu_{\rm rel}$, where $\mu_{\rm rel}$ is the relative source–lens proper motion, and the microlensing parallax, $\pi_E = (\pi_L - \pi_S)/\theta_E$. Precise, multiepoch astrometry can measure θ_E directly and combined with photometry to measure the lens mass, $M_L = \theta_E/\kappa\pi_E$.

Over the past 25 years, numerous photometric microlensing surveys have been conducted to search for a wide variety of lenses, including massive astrophysical compact halo objects (MACHOs) that might make up dark matter, stars of all masses, and, most recently, exoplanets (Paczynski 1986, 1991; Griest et al. 1991; Mao & Paczynski 1991). Current ground-based microlensing surveys such as the Optical Gravitational Lensing Experiment (OGLE, Udalski et al. 1994), Microlensing Observations in Astrophysics (MOA, Bond et al. 2001), and Korea Microlensing Telescope Network (KMTNet; Kim et al. 2016) monitor hundreds of millions of stars toward the Galactic bulge, identifying thousands of photometric microlensing events each year. Photometry-only searches for stellar-mass BHs have been attempted (e.g., Bennett et al. 2002; Mao et al. 2002, 2016) but have only been able to identify BH candidates or place loose statistical constraints on the BH mass function.

In contrast to the now-routine measurements of photometric microlensing, detections of astrometric microlensing are still at the forefront of our technical capabilities (Lu et al. 2016; Kains et al. 2017; Rybicki et al. 2018). Only a handful of astrometric measurements of the gravitational deflection of light have ever been made, all for nearby (<10 pc) lenses that were astrometrically anticipated (Eddington 1919; Sahu et al. 2017; Zurlo et al. 2018) and none of which were BHs.

If there are 10^8 BHs in the Milky Way, they should contribute only about 0.1% to the stellar mass of the Milky Way. In contrast, they would make up around 1% of the Milky Way's microlensing events due to their larger lensing cross section. Thus, of the thousands of microlensing events detected each year, a few tens should be due to BHs (Gould 2000; Lam et al. 2020). However, a 1% detection rate is akin to looking for BH needles in a Galactic haystack. By limiting to long-duration microlensing events with $t_E > 120$ days, the probability of a microlensing event being a BH rises to ∼40% (Lam et al. 2020).

We present a joint photometric and astrometric analysis of five candidate BH microlensing events. We briefly summarize the observations in Section 2 and methods in Section 3. A large nonlinear astrometric microlensing signal was detected in one of the five candidates named OGLE-2011-BLG-0462/MOA-2011-BLG-191 (OB110462 for short) consistent with a compact-object lens. The resulting mass-gap BH or NS nature of OB110462 is presented in Section 4 and discussed in a broader context in Section 5. Final conclusions are presented in Section 6. A complete description of the observations, methods, and detailed results and discussion for all five targets is presented in the Supplemental Materials within Lam et al. (2022).

2. Observations and Analysis

Five BH candidate microlensing events were first identified photometrically in the OGLE-IV (Udalski et al. 2015) and MOA (Hearnshaw et al. 2006; Sumi 2008) Galactic Bulge surveys. The target discussed in detail here is OB110462, which is located at (17:51:40.19,−29:53:26.3) toward the Galactic bulge. The remaining target properties are described in Supplemental Section 3.1 of Lam et al. (2022).

The photometric light curves for each candidate span 7 to 11 yr, with approximately daily cadence except for seasonal gaps from November to February and photometric precision of ∼2% for each measurement. Astrometric observations were obtained with the Hubble Space Telescope (HST) in the F606W (V-band) and F814W (I-band) filters. Astrometric monitoring began around each event's photometric peak with a typical cadence of 1–2 times a year and an astrometric precision of ∼0.3 mas per epoch. A more detailed description of the observations, data analysis, and multiepoch astrometric alignment is presented in Supplemental Sections 3 and 4 of Lam et al. (2022).

3. Modeling Methods

To measure the physical properties of the lens and source for each event, we simultaneously fit the ground-based photometry and HST photometry and astrometry with a point-source, point-lens (PSPL) microlensing model including source and lens parallax. All microlensing quantities defined in this work are in the heliocentric reference frame. The model parameters describing the lensing geometry include t_E and π_E as described in Section 1 as well as the time (t_0) and distance (u_0) of the closest projected approach between the source and lens in the heliocentric frame and the direction of the microlensing parallax vector $\boldsymbol{\pi}_E$. The direction of $\boldsymbol{\pi}_E$ is defined to be the same as the direction of the source–lens relative proper motion vector[19], i.e., $\boldsymbol{\pi}_E \| \boldsymbol{\mu}_{\rm rel}$. For each photometric filter, the baseline brightness ($m_{\rm base}$) and source flux fraction (or blend parameter, $b_{\rm SFF}$) are fit. We also fit the astrometric model parameters θ_E and the source's parallax (π_S), position at t_0 ($\boldsymbol{x}_{S0}$), and proper motion on the sky ($\boldsymbol{\mu}_S$). A complete description of the microlens model is presented in Supplemental Section 5.1 of Lam et al. (2022).

[19] Note that we define $\boldsymbol{\mu}_{\rm rel}$ to be the source–lens relative proper motion (Supplementary Section 5.1) following the convention of astrometric microlensing papers (e.g., Hog et al. 1995; Miyamoto & Yoshii 1995; Lu et al. 2016), while the exoplanet microlensing community typically defines $\boldsymbol{\mu}_{\rm rel}$ to be the lens–source relative proper motion.

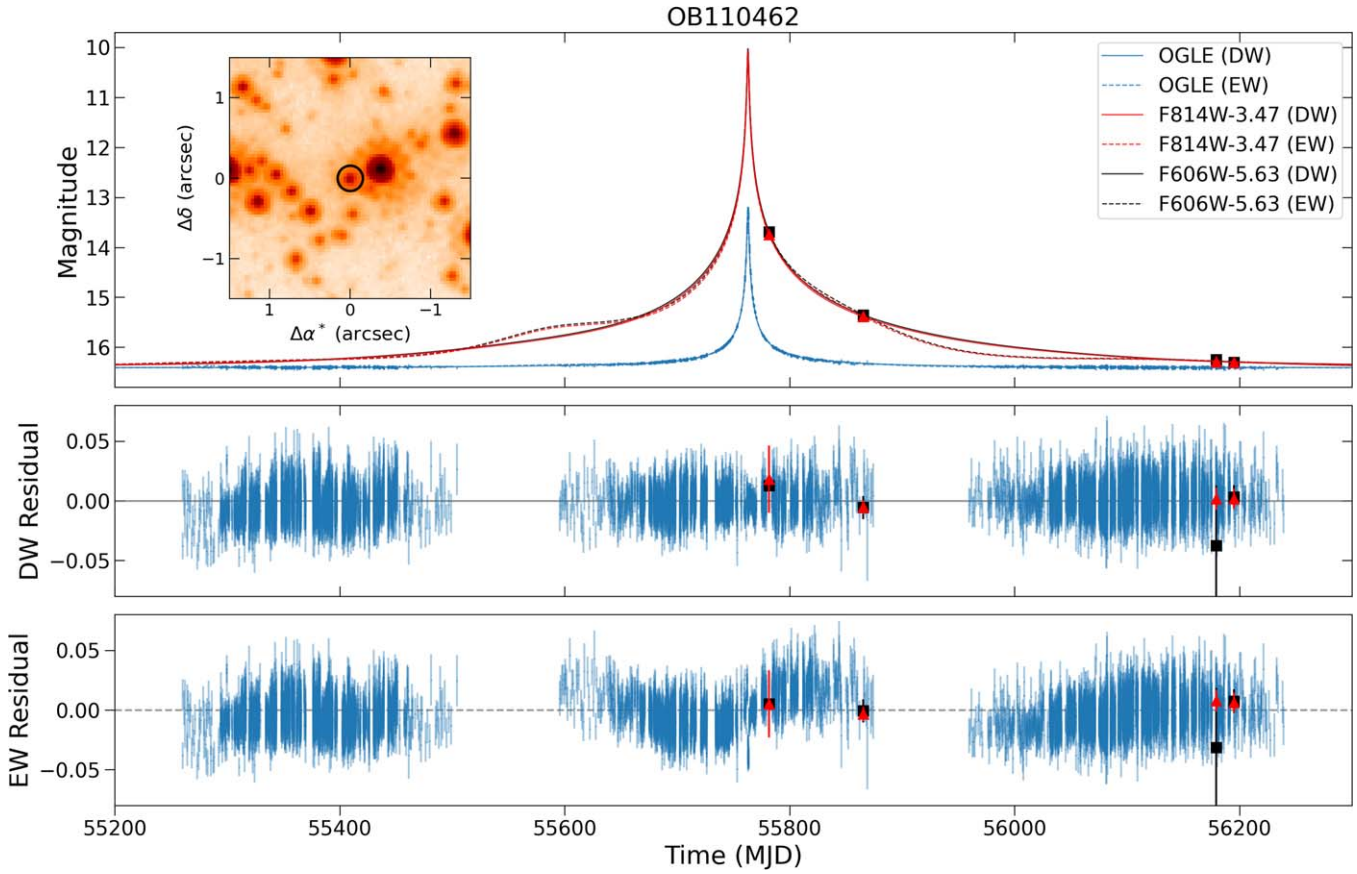

Figure 1. HST image (inset) and photometric light curve (top) for OB110462. In the image, OB110462 is circled in black and is shown in its unmagnified state. Observations are shown as points in blue (OGLE), red, and black (HST). The default-weighted (DW; solid) and equal-weighted (EW; dashed) maximum likelihood models are shown along with their corresponding residuals (DW: middle, EW: bottom). See Supplemental Section 5.3 of Lam et al. (2022) for more details on the two different models.

The best-fit model parameters and uncertainties are estimated using Bayesian inference and the `MultiNest` nested sampling routine (Feroz et al. 2009; Skilling 2004; see Supplemental Section 5 of Lam et al. 2022 for details). There is some tension between the preferred model parameters by the photometry versus astrometry data for OB110462. When using the default weight (DW) likelihood where each data point and corresponding measurement uncertainty contribute equally to the likelihood, the photometry dominates as it has $>100\times$ more data points than the astrometry data set. We also fit models with a likelihood that gives equal weight (EW) to each independent data set (see Supplemental Section 5.3 of Lam et al. 2022 for details). With the EW likelihood, the astrometry has much more constraining power. Results from both models are described in Section 4.

4. Results

A large (>1 mas) astrometric microlensing signal is detected in OB110462 (Section 4.1). The four other candidates are presented in Supplemental Section 7 of Lam et al. (2022) and either show no significant astrometric microlensing signal or have a low lens mass inconsistent with a black hole.

4.1. OB110462

From the microlensing fit, we infer that OB110462 is an NS or a mass-gap BH, depending on the likelihood function adopted (see Supplemental Section 5.3 of Lam et al. 2022). The data and model for OB110462 with the DW likelihood are shown in Figures 1 (photometry) and 2 (astrometry), and the fit posteriors are summarized in Table 1. The mass posteriors of the lens are shown in Figure 3. The inferred Einstein crossing time t_E is $280.87^{+6.54}_{-5.96}$ days, the microlensing parallax π_E is $0.12^{+0.01}_{-0.01}$, the Einstein radius θ_E is $3.89^{+1.12}_{-1.16}$, and the lens mass M_L is $3.79^{+0.62}_{-0.57} M_\odot$. The data and model for OB110462 with the EW likelihood are shown in Figures 1 (photometry) and 2 (astrometry), and the fit posteriors are summarized in Table 2. The inferred Einstein crossing time t_E is $278.56^{+12.52}_{-9.16}$ days, the microlensing parallax π_E is $0.24^{+0.05}_{-0.05}$, the Einstein radius θ_E is $4.13^{+0.96}_{-0.91}$, and the lens mass M_L is $2.15^{+0.67}_{-0.54} M_\odot$. Further, we find that the object is located relatively nearby at 0.70–1.92 kpc in the direction of the Galactic bulge and has a small transverse velocity of <30 km s^{-1}. Figure 4 shows the on-sky lensing geometry of OB110462 inferred from the DW and EW likelihood models, showing the relative motions of the source and lens with respect to each other.

The probability that OB110462 is a dark lens is 100%, ruling out the possibility of a stellar lens and making OB110462 the first detection of a compact object with astrometric microlensing. Assuming there is a transition from white dwarfs to neutron stars at $1.2 M_\odot$ and neutron stars to BHs at $2.2 M_\odot$, the relative probabilities of WD:NS:BH are 0:0:100 for the DW fit and 6:50:44 for the equally weighted (EW) fit.

The microlensing fit also yields information about the distance and transverse velocity of the lens. The lens is

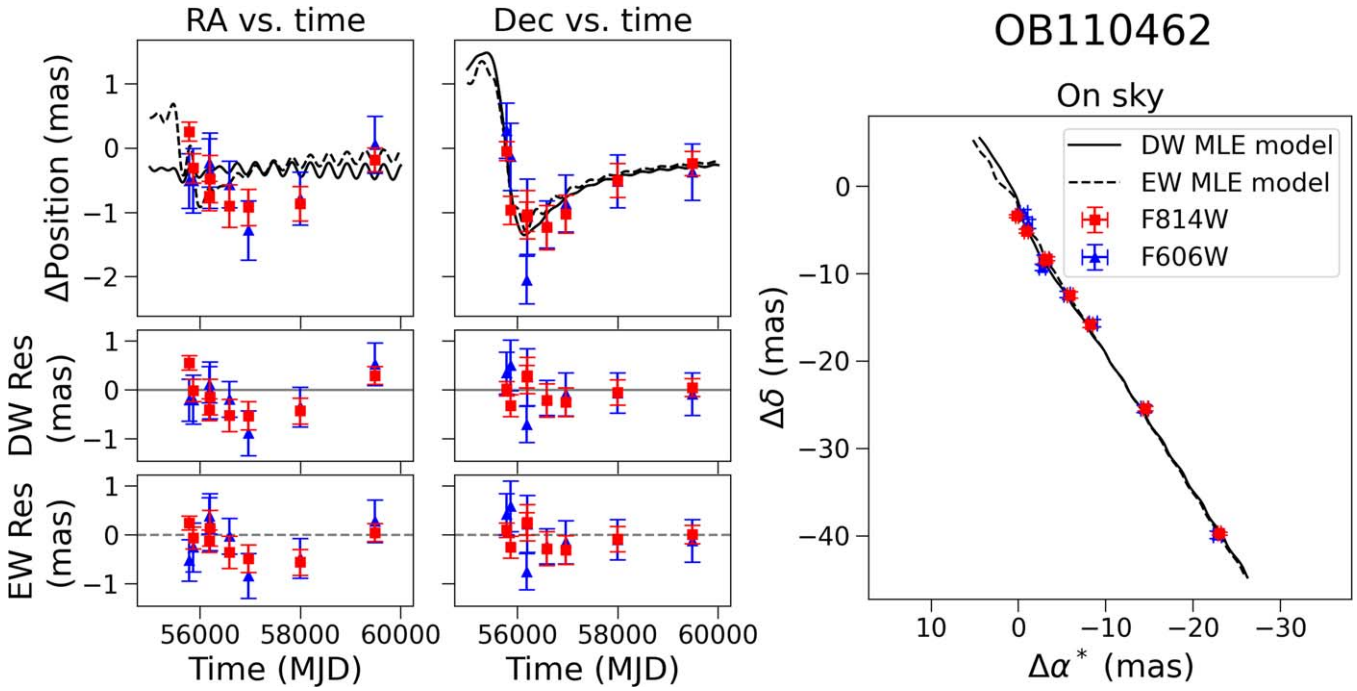

Figure 2. OB110462 astrometry, using the DW (solid) and EW (dashed) likelihoods. Left column, top to bottom: R.A. ($\Delta\alpha^*$) vs. time with source's unlensed motion subtracted; residuals to the maximum likelihood (MLE) model for $\Delta\alpha^*$ vs. time fit. HST F814W astrometry data are shown in red; HST F606W astrometry data are shown in blue. The MLE model is shown in black. Middle column, top to bottom: same as the left column, except decl. ($\Delta\delta$) instead of $\Delta\alpha^*$. Right panel: astrometry as seen on sky, in the barycentric frame. OB110462 shows a strong >1 mas, nonlinear astrometric microlensing signal.

relatively nearby at a distance of 1.47–1.92 kpc or 0.70–1.30 kpc for the DW and EW solutions, respectively. The inferred lens velocity is $<30\,\mathrm{km\,s^{-1}}$ for both solutions with a slower velocity of 2–12 $\mathrm{km\,s^{-1}}$ from the EW solution and a faster velocity of 21–27 $\mathrm{km\,s^{-1}}$ from the DW solution. In both cases, the velocities appear consistent with the compact object receiving little to no kick, although the line-of-sight velocity is not measurable from these observations.

Based on an analysis of the source position in the CMD, the OB110462 source star is around the main-sequence turnoff on the redder and more luminous side of the main sequence, suggesting it is most likely a giant or subgiant star. However, a main-sequence source could still be consistent. The relative proper motion and parallax also favor a star on the near side of the Bulge (see Supplemental Section 7.6 of Lam et al. 2022 for more details).

A point-source, point-lens (PSPL) model is not the end of the story for OB110462. There is no PSPL model that can simultaneously fit both the photometry and the astrometry. Specifically, the direction of $\mu_{\rm rel}$ preferred by photometry and astrometry are different. The best-fit PSPL model for the DW likelihood fits the photometry very well but leaves a significant ~0.5 mas coherent astrometric residual in R.A. (Figure 2). The best-fit PSPL model for the EW likelihood leaves a significant and coherent ~0.03 mag residual in the photometry, but fits the astrometry in RA better than the DW likelihood model, although some unexplained astrometric residuals still remain. More complex microlensing geometry models, such as those involving a binary source or lens, should be explored. As mentioned in Supplemental Section 4.2.5 of Lam et al. (2022), we apply a constant positional offset to the F606W data in order to make it match up with the F814W data. However, this filter-dependent positional difference may actually be astrophysical and consistent with a small contribution from a faint companion to the source. Either way, both solutions indicate an NS or BH detection.

The alternative explanation to the tension between the photometry and astrometry of OB110462 is some type of systematic error in one or both sets of observations. This possibility is discussed in Supplemental Section 8.3 of Lam et al. (2022).

4.2. Is OB110462 a BH or an NS?

One means of further understanding the BH or NS nature of OB110462 would be to detect electromagnetic radiation from the lens. We searched existing X-ray and pulsar catalogs at the position of OB110462 and did not find any counterpart (see Supplemental Section 5 of Lam et al. (2022) for details). Unfortunately, OB110462 is not in the Gaia EDR3 catalog as it is too faint.

Future observations of OB110462 will be useful to determine its true nature. Continued astrometric monitoring, including the remaining data from HST Cycle 29 program GO-16760 (Lam & Lu 2021) will continue to improve the lens mass estimate as described in Supplemental Section 5 of Lam et al. (2022). High contrast imaging observations in the next 5–10 yr would also be worthwhile. If the lens is indeed a solitary NS or BH, lack of an optical/infrared lens detection would bolster support of the dark isolated lens interpretation but be unable to distinguish between NS or BH as the relative proper motion differentiating the DW and EW solutions cannot be measured in the case of a dark lens. In that case, only a deep, targeted X-ray observation could help in differentiating between the NS versus BH scenarios. On the other hand, optical/infrared detection of a lens separate from the source would point to a binary lens scenario. Binary source or binary lens models can be further explored through precision radial velocity searches.

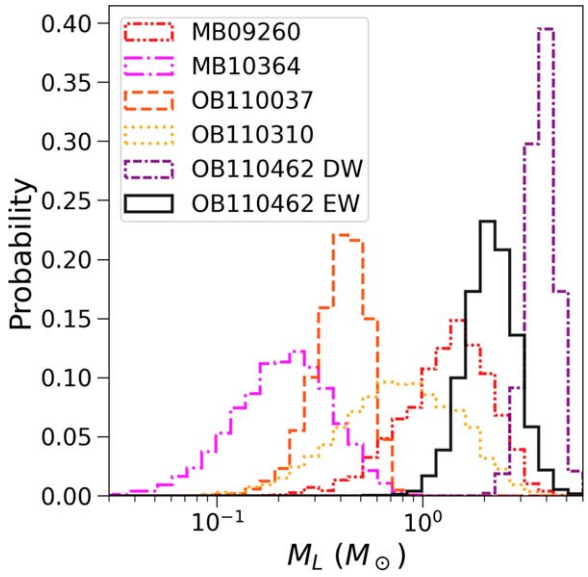

Figure 3. Lens-mass posterior probabilities for the five microlensing BH candidates. Two mass posteriors are shown for OB110462, one for each model (DW and EW). See Supplemental Section 5.3 of Lam et al. (2022) for details on the two models. MB09260, MB10364, OB110037, and OB110310 are discussed in detail in the Supplemental paper.

Table 1
OB110462 DW Fit Values

Parameter	Med$^{+1\sigma}_{-1\sigma}$	MAP	MLE
t_0 (MJD)	$55761.07^{+0.99}_{-0.96}$	55760.65	55759.15
u_0	$-0.06^{+0.006}_{-0.009}$	−0.06	−0.07
t_E (days)	$280.87^{+6.54}_{-5.96}$	284.94	277.47
$\log_{10}(\theta_E/\mathrm{mas})$	$0.59^{+0.05}_{-0.07}$	0.47	0.60
π_S (mas)	$0.11^{+0.02}_{-0.02}$	0.12	0.12
$\pi_{E,E}$	$0.010^{+0.005}_{-0.004}$	0.009	0.0007
$\pi_{E,N}$	$-0.12^{+0.01}_{-0.01}$	−0.12	−0.14
$x_{S0,E}$ (mas)	$229.75^{+0.07}_{-0.08}$	229.82	229.80
$x_{S0,N}$ (mas)	$-214.28^{+0.11}_{-0.13}$	−214.58	−214.22
$\mu_{S,E}$ (mas yr^{-1})	$-2.25^{+0.02}_{-0.02}$	−2.25	−2.25
$\mu_{S,N}$ (mas yr^{-1})	$-3.57^{+0.02}_{-0.02}$	−3.55	−3.57
$b_{\mathrm{SFF},O}$	$0.05^{+0.0004}_{-0.0004}$	0.05	0.05
$m_{\mathrm{base},O}$ (mag)	$16.41^{+0.0001}_{-0.0001}$	16.41	16.41
$b_{\mathrm{SFF},H8}$	$0.90^{+0.02}_{-0.02}$	0.89	0.91
$m_{\mathrm{base},H8}$ (mag)	$19.86^{+0.006}_{-0.006}$	19.86	19.87
$b_{\mathrm{SFF},H6}$	$0.94^{+0.02}_{-0.02}$	0.95	0.94
$m_{\mathrm{base},H6}$ (mag)	$22.04^{+0.009}_{-0.009}$	22.05	22.04
M_L ($M_\odot$)	$3.79^{+0.62}_{-0.57}$	3.01	3.58
π_L (mas)	$0.60^{+0.08}_{-0.08}$	0.48	0.67
π_{rel} (mas)	$0.48^{+0.08}_{-0.08}$	0.36	0.55
$\mu_{L,E}$ (mas yr^{-1})	$-2.64^{+0.18}_{-0.24}$	−2.54	−2.28
$\mu_{L,N}$ (mas yr^{-1})	$1.46^{+0.63}_{-0.71}$	0.26	1.69
$\mu_{\mathrm{rel},E}$ (mas yr^{-1})	$0.40^{+0.23}_{-0.19}$	0.28	0.03
$\mu_{\mathrm{rel},N}$ (mas yr^{-1})	$-5.02^{+0.71}_{-0.64}$	−3.81	−5.26
θ_E (mas)	$3.89^{+1.12}_{-1.16}$	2.98	4.00
π_E	$0.12^{+0.01}_{-0.01}$	0.14	0.13
$\delta_{c,\max}$ (mas)	$1.37^{+0.40}_{-0.41}$	1.05	1.41

Note. The columns list the median $\pm1\sigma$ (68%) credible intervals, maximum a posteriori (MAP) solution, and maximum likelihood estimator (MLE) solution.

Table 2
OB110462 EW Fit Values

Parameter	Med$^{+1\sigma}_{-1\sigma}$	MAP	MLE
t_0 (MJD)	$55747.17^{+7.36}_{-7.55}$	55735.10	55735.10
u_0	$-0.11^{+0.02}_{-0.01}$	−0.13	−0.13
t_E (days)	$278.56^{+12.52}_{-9.16}$	267.37	267.37
$\log_{10}(\theta_E/\mathrm{mas})$	$0.62^{+0.09}_{-0.11}$	0.60	0.60
π_S (mas)	$0.11^{+0.02}_{-0.02}$	0.10	0.10
$\pi_{E,E}$	$-0.07^{+0.05}_{-0.05}$	−0.15	−0.15
$\pi_{E,N}$	$-0.23^{+0.05}_{-0.03}$	−0.29	−0.29
$x_{S0,E}$ (mas)	$229.97^{+0.16}_{-0.17}$	230.07	230.07
$x_{S0,N}$ (mas)	$-214.31^{+0.21}_{-0.21}$	−214.37	−214.37
$\mu_{S,E}$ (mas yr^{-1})	$-2.25^{+0.03}_{-0.03}$	−2.24	−2.24
$\mu_{S,N}$ (mas yr^{-1})	$-3.56^{+0.03}_{-0.03}$	−3.57	−3.57
$b_{\mathrm{SFF},O}$	$0.05^{+0.003}_{-0.004}$	0.06	0.06
$m_{\mathrm{base},O}$ (mag)	$16.41^{+0.007}_{-0.007}$	16.41	16.41
$b_{\mathrm{SFF},H8}$	$0.95^{+0.05}_{-0.06}$	0.99	0.99
$m_{\mathrm{base},H8}$ (mag)	$19.88^{+0.008}_{-0.007}$	19.88	19.88
$b_{\mathrm{SFF},H6}$	$0.99^{+0.04}_{-0.06}$	1.04	1.04
$m_{\mathrm{base},H6}$ (mag)	$22.04^{+0.01}_{-0.01}$	22.03	22.03
M_L ($M_\odot$)	$2.15^{+0.67}_{-0.54}$	1.51	1.51
π_L (mas)	$1.09^{+0.34}_{-0.32}$	1.38	1.38
π_{rel} (mas)	$0.98^{+0.34}_{-0.32}$	1.27	1.27
$\mu_{L,E}$ (mas yr^{-1})	$-0.69^{+0.91}_{-0.94}$	0.25	0.25
$\mu_{L,N}$ (mas yr^{-1})	$1.53^{+1.21}_{-1.12}$	1.22	1.22
$\mu_{\mathrm{rel},E}$ (mas yr^{-1})	$-1.56^{+0.95}_{-0.91}$	−2.49	−2.49
$\mu_{\mathrm{rel},N}$ (mas yr^{-1})	$-5.08^{+1.13}_{-1.22}$	−4.79	−4.79
θ_E (mas)	$4.13^{+0.96}_{-0.91}$	3.95	3.95
π_E	$0.24^{+0.05}_{-0.05}$	0.32	0.32
$\delta_{c,\max}$ (mas)	$1.46^{+0.34}_{-0.32}$	1.40	1.40

4.3. Number of Detected BHs

Next, we compare our observed BH yield to the theoretical expectation calculated using the PopSyCLE simulations. PopSyCLE's Galactic model contains 2×10^8 BHs ranging from 5 to $16M_\odot$ (Lam et al. 2020). For a sample of simulated events that would be observable by OGLE (see Table 4 of Lam et al. 2020), we calculate the fraction of those events due to BHs as a function of the Einstein crossing time t_E as described in Supplemental Section 7.9 in Lam et al. (2022). Figure 5 shows the expectation of detecting $N_{\mathrm{BH}} = 0$, 1, …, 5 BHs within our sample of 5 targets. The probability of detecting zero or one BH in our simulation is ∼25% and ∼45%, respectively. This estimate is consistent with our single detection of an NS–BH object. Note that in PopSyCLE, there are no $2-5M_\odot$ mass-gap NSs or BHs in the simulation, and hence no exact OB110462 analog.

5. Discussion

OB110462 is the first definitive detection of a compact object discovered with astrometric microlensing. Depending on the likelihood function used to evaluate the fit (see Supplemental Section 5.3 of Lam et al. 2022), it is either an NS (50% probability for the EW likelihood), a BH (44% probability for the EW likelihood, 100% probability for the DW likelihood), or a white dwarf (6% probability for the EW likelihood). The other four candidates discussed in detail in Supplemental Section 7 of Lam et al. (2022) are mostly likely stars, white

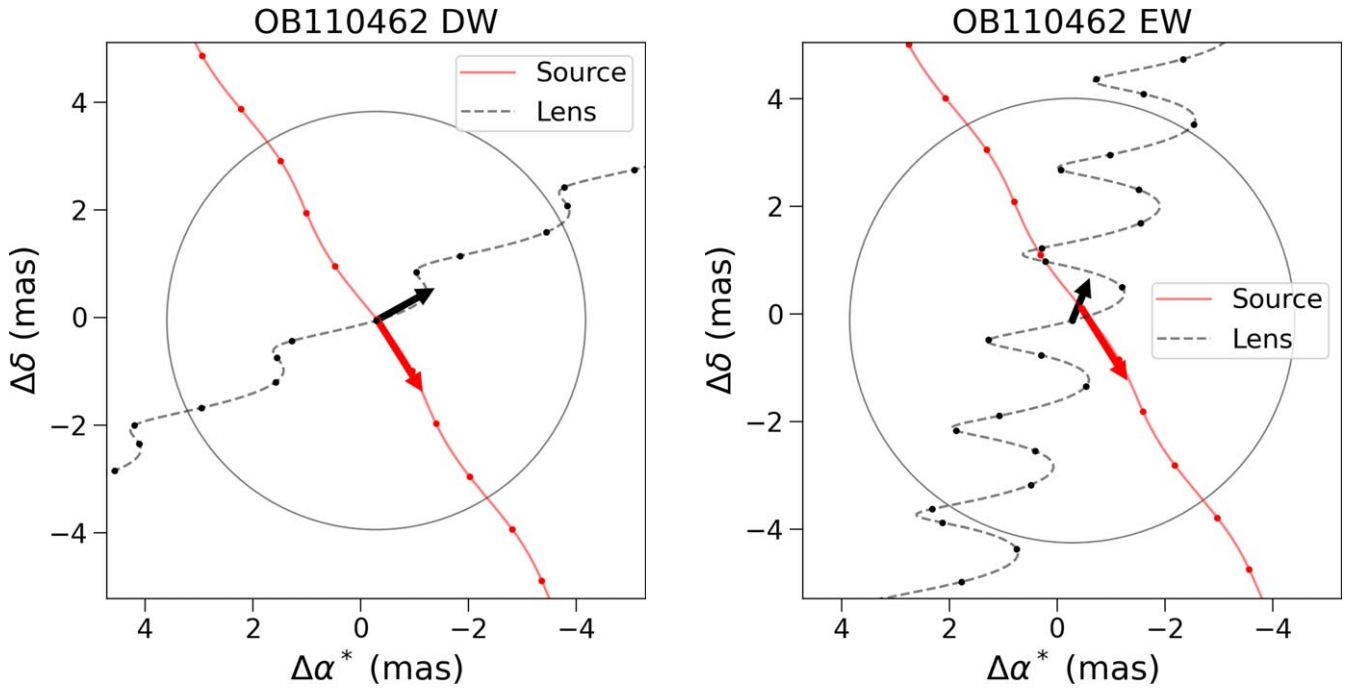

Figure 4. On-sky lensing geometry of OB110462 showing the resolved motion of the lens and source, as inferred from the default-weight (DW) model (left) and the equal-weight (EW) model (right); see Supplemental Section 5.3 of Lam et al. (2022) for details about the different models. The Einstein ring is shown as a gray circle of radius θ_E. The solid red line shows the trajectory of the source, while the dashed black line shows the trajectory of the lens. Note that the red line shows the unlensed position or the source and not the centroid of the source's lensed images. The dots on top of the trajectories are spaced at intervals of 100 days. The red and black arrows indicate the proper motion of the source and lens, respectively. The tail of the arrow is at the location of the source and lens at time t_0; the length of the arrows is proportional to the magnitude of the source and lens proper motions.

dwarfs, or neutron stars, although an NS–BH mass-gap object cannot be ruled out in two cases.

Here we discuss the observed BH yield compared to theoretical expectations (Section 5.1) and the implications for the BH mass function (Section 5.2).

5.1. Comparison to Simulations

5.1.1. π_E–t_E–$\delta_{c,max}$

As described in Lam et al. (2020), BH candidates can be identified photometrically by their long t_E and small π_E, and confirmed astrometrically by measuring the maximum astrometric shift $\delta_{c,\max} = \theta_E/\sqrt{8}$ (see Supplemental Section 5.1). Figure 6 shows the $1\sigma-2\sigma-3\sigma$ posterior contours of π_E versus t_E (left) and π_E versus $\delta_{c,\max}$ (right) of the microlensing models for the five targets, compared against simulated microlensing events generated by the `PopSyCLE` software (Lam et al. 2020). By comparing the π_E-t_E and $\pi_E-\delta_{c,\max}$ posteriors against the simulation, we can gain a more intuitive understanding of the inferred lens types for the targets (Supplemental Table 9 of Lam et al. 2022).

Both EW and DW models for OB110462 fall solidly within the $2-5M_\odot$ mass gap shown in the $\pi_E-\delta_{c,\max}$ parameter space. Because the EW solution leads to a larger and more uncertain value of π_E than the DW solution, an NS or even white dwarf lens is a possibility. On the other hand, the DW solution prefers a smaller and more well-constrained value of π_E than the EW solution, leading to a much more definitive solution of a mass-gap BH. However, both the EW and DW solutions for OB110462 fall in a somewhat unusual part of the π_E-t_E parameter space for BHs: typical BH π_E are around 0.02, while for OB110462, π_E is around 0.1. This is because `PopSyCLE` simulations only contain BHs with masses from $\sim 5-16M_\odot$; if OB110462 is truly a mass-gap BH, it would not correspond to any BHs in the simulation.

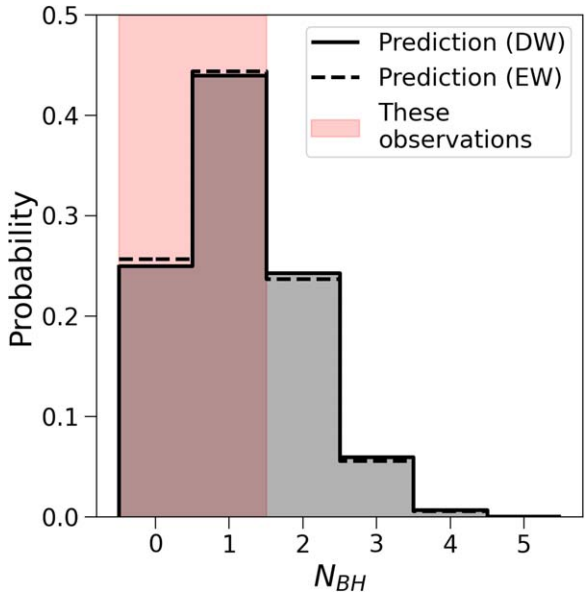

Figure 5. Probability of detecting N BHs as calculated from the `PopSyCLE` simulation. Two predictions are shown, depending on the likelihood used for OB110462 (DW or EW)). See Supplemental Section 5.3 of Lam et al. (2022) for details on the two models. Our observation of 0 or 1 BHs is consistent with either OB110462 model prediction.

5.2. OB110462 in Comparison to the BH Population

Several attempts have been made to determine the Milky Way BH mass function using dynamical mass measurements of

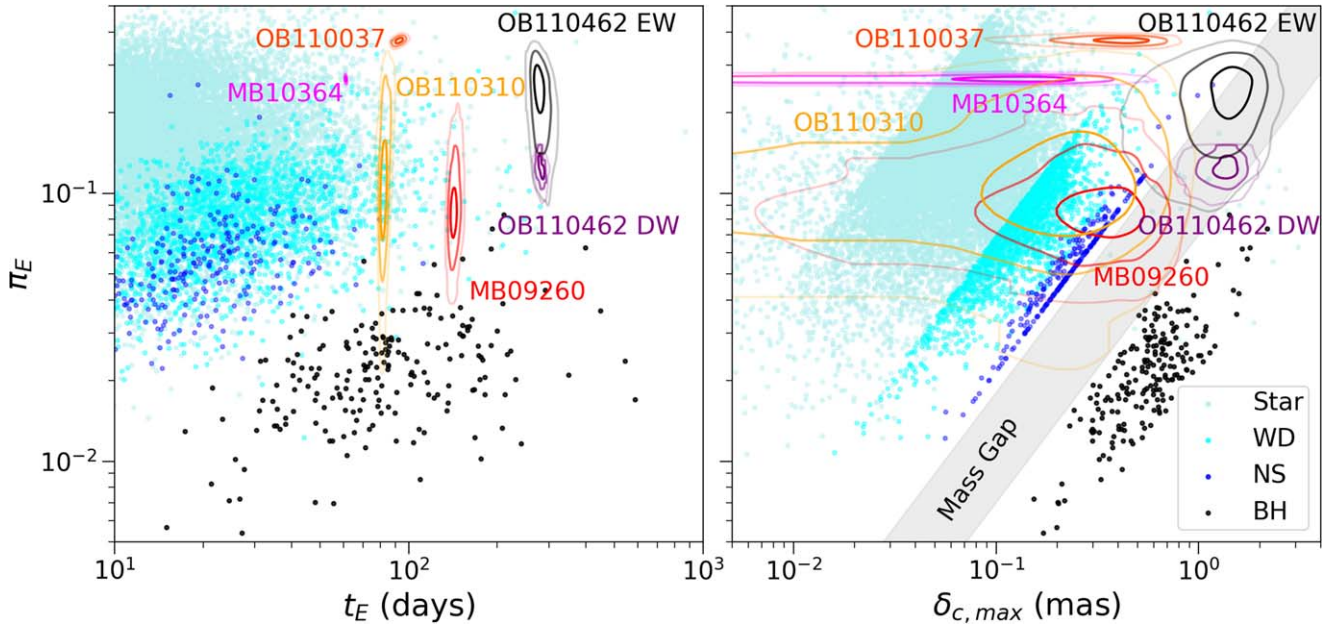

Figure 6. Microlensing parallax π_E vs. Einstein crossing time t_E (left) and maximum astrometric shift $\delta_{c,\max}$ (right). Points are from the PopSyCLE simulation. Contours are $1\sigma-2\sigma-3\sigma$ (39.3–86.5–98.9%) credible regions from the microlensing model fits to the five BH candidates. There are two fits for OB110462 (DW and EW; see Supplemental Section 5.3 of Lam et al. 2022 for details). The OB110462 DW solution has a smaller π_E than the OB110462 EW solution and has a correspondingly more massive lens mass. Both solutions fall solidly in the NS–BH mass gap, making OB110462 the best BH candidate. MB09260 and OB110310 are most likely white dwarfs or NSs, although due to the uncertainty in π_E and $\delta_{c,\max}$ higher- and lower-mass lenses cannot be definitively ruled out. OB110037 and MB10364 are not BHs as they have very large π_E, as well as relatively short t_E and small $\delta_{c,\max}$. MB09260, MB10364, OB110037, and OB110310 are discussed in detail in the Supplemental paper.

BHs in binaries. The mass gap between 3 and 5 $M_\odot$ was first observed in low-mass X-ray binaries (Bailyn et al. 1998; Özel et al. 2010; Farr et al. 2011). However, more recent detections of BHs in this mass range from both gravitational wave mergers and in non-interacting binaries suggests that the mass gap may actually be filled with BHs (e.g., Abbott et al. 2017; Thompson et al. 2019). For a complete description of the Milky Way BHs found to date, see Supplemental Section 8.1 of Lam et al. (2022). If OB110462 is a BH, it too shows that the mass function of BHs extends into the mass-gap regime.

It is somewhat surprising that massive BHs have not been found in our microlensing search as well as in searches for BHs in wide binaries (Thompson et al. 2019; Rowan et al. 2021; El-Badry et al. 2022). Both microlensing and radial velocity searches should be biased toward finding 10 $M_\odot$ objects more easily than 3 $M_\odot$ objects as described in Supplemental Section 8.1 of Lam et al. (2022). It may be that the selection bias is offset by the steep mass function for massive stars and thus BHs. As the sample of BHs in the Milky Way grows, a more quantitative analysis of the sample selection will be essential to constrain the true BH mass function.

6. Conclusion

We analyze five microlensing events with candidate BH lenses. Combining HST astrometry and densely sampled ground-based photometry, we derive masses for these five lenses as well as their probability of being a BH. Of the five targets, we make one definitive >1 mas detection of astrometric microlensing (OB110462). The mass of the lens in OB110462 is in the range 1.6–4.4 $M_\odot$, making it the first detection of a compact object through astrometric microlensing.

We use our detection of a mass-gap BH or NS and the nondetections of BHs in the rest of the sample to observationally constrain the number of BHs in the Milky Way. Our observational BH yield currently agrees with simulations assuming 2×10^8 BHs in the Milky Way, albeit with very large uncertainties due to the small sample size. The ability to place more stringent constraints on the number and mass distribution of Galactic BHs will require larger samples, such as those that may be delivered by the Roman Space Telescope's microlensing survey.

Astrometric microlensing holds the key to uncovering the hidden BH population. Further pursuit and refinement of the event selection, observing, and modeling process will fulfill the full promise of this technique and its ability to reveal the properties of Galactic BHs.

Shortly prior to this work being submitted for review, we learned of an independent analysis of OB110462 carried out by Sahuet al. (2022). Notably, they reach a different conclusion about the mass of the lens ($7.1 \pm 1.3 M_\odot$). It is not clear whether the discrepancy is due to the use of different data sets (e.g., we include an additional epoch of 2021 HST data), performing the analysis differently (e.g., we explore solutions allowed by both photometry and astrometry using different likelihood weights), or a combination of both. In addition, although both analyses make clear detections of an astrometric deflection, the direction of the deflections are in opposing directions in RA. Preliminary work shows that different choice of reference stars across the two teams is not the source of the discrepancy. However, significant further work is required to fully understand the differences between the two analyses.

The light curves and astrometry of the five candidates, the microlensing model posteriors of the candidates, as well as the simulation outputs used to interpret the data are publicly available on Zenodo at https://doi.org/10.5281/zenodo.6607578 (DOI: 10.5281/zenodo.6607578).

See the Supplement of Lam et al. (2022) for a full list of acknowledgments.

ORCID iDs

Casey Y. Lam https://orcid.org/0000-0002-6406-1924
Jessica R. Lu https://orcid.org/0000-0001-9611-0009
Andrzej Udalski https://orcid.org/0000-0001-5207-5619
David P. Bennett https://orcid.org/0000-0001-8043-8413
Jan Skowron https://orcid.org/0000-0002-2335-1730
Przemek Mróz https://orcid.org/0000-0001-7016-1692
Radek Poleski https://orcid.org/0000-0002-9245-6368
Takahiro Sumi https://orcid.org/0000-0002-4035-5012
Szymon Kozłowski https://orcid.org/0000-0003-4084-880X
Paweł Pietrukowicz https://orcid.org/0000-0002-2339-5899
Igor Soszyński https://orcid.org/0000-0002-7777-0842
Krzysztof Ulaczyk https://orcid.org/0000-0001-6364-408X
Łukasz Wyrzykowski https://orcid.org/0000-0002-9658-6151
Shota Miyazaki https://orcid.org/0000-0001-9818-1513
Naoki Koshimoto https://orcid.org/0000-0003-2302-9562
Nicholas J. Rattenbury https://orcid.org/0000-0001-5069-319X
Matthew W. Hosek, Jr. https://orcid.org/0000-0003-2874-1196
Richard Barry https://orcid.org/0000-0003-4916-0892
Akihiko Fukui https://orcid.org/0000-0002-4909-5763
Yuki Hirao https://orcid.org/0000-0003-4776-8618
Yoshitaka Itow https://orcid.org/0000-0002-8198-1968
Iona Kondo https://orcid.org/0000-0002-3401-1029
Yasushi Muraki https://orcid.org/0000-0003-1978-2092
Greg Olmschenk https://orcid.org/0000-0001-8472-2219
Clément Ranc https://orcid.org/0000-0003-2388-4534
Yuki Satoh https://orcid.org/0000-0002-1228-4122
Aikaterini Vandorou https://orcid.org/0000-0002-9881-4760
Natasha S. Abrams https://orcid.org/0000-0002-0287-3783
Sam Rose https://orcid.org/0000-0003-4725-4481
Sean K. Terry https://orcid.org/0000-0002-5029-3257

References

Abbott, B. P., Abbott, R., Abbott, T. D., et al. 2017, ApJL, 851, L16
Abbott, R., Abbott, T. D., Abraham, S., et al. 2020, ApJL, 896, L44
Agol, E., Kamionkowski, M., Koopmans, L. V. E., & Blandford, R. D. 2002, ApJL, 576, L131
Bailyn, C. D., Jain, R. K., Coppi, P., & Orosz, J. A. 1998, ApJ, 499, 367
Belczynski, K., Sadowski, A., & Rasio, F. A. 2004, ApJ, 611, 1068
Bennett, D. P., Becker, A. C., Quinn, J. L., et al. 2002, ApJ, 579, 639
Bond, I. A., Abe, F., Dodd, R. J., et al. 2001, MNRAS, 327, 868
Corral-Santana, J. M., Casares, J., Muñoz-Darias, T., et al. 2016, A&A, 587, A61
Eddington, A. S. 1919, Obs, 42, 119
El-Badry, K., Seeburger, R., Jayasinghe, T., et al. 2022, MNRAS, 512, 5620
Farr, W. M., Sravan, N., Cantrell, A., et al. 2011, ApJ, 741, 103
Fender, R. P., Maccarone, T. J., & Heywood, I. 2013, MNRAS, 430, 1538
Feroz, F., Hobson, M. P., & Bridges, M. 2009, MNRAS, 398, 1601
Gould, A. 2000, ApJ, 535, 928
Griest, K., Alcock, C., Axelrod, T. S., et al. 1991, ApJL, 372, L79
Hearnshaw, J. B., Abe, F., Bond, I. A., et al. 2006, in The 9th Asian-Pacific Regional IAU Meeting, ed. W. Sutantyo et al. (Bandung: ITB Press), 272
Hog, E., Novikov, I. D., & Polnarev, A. G. 1995, A&A, 294, 287
Kains, N., Calamida, A., Sahu, K. C., et al. 2017, ApJ, 843, 145
Kim, S.-L., Lee, C.-U., Park, B.-G., et al. 2016, JKAS, 49, 37
Lam, C., & Lu, J. R. 2021, HST Proposal, 29, 16760
Lam, C. Y., Lu, J. R., Hosek, M. W. J., Dawson, W. A., & Golovich, N. R. 2020, ApJ, 889, 31
Lam, C. Y., Lu, J. R., Udalski, A., et al. 2022, arXiv:2202.01903
Lu, J. R., Sinukoff, E., Ofek, E. O., Udalski, A., & Kozlowski, S. 2016, ApJ, 830, 41
Mao, S., & Paczynski, B. 1991, ApJL, 374, L37
Mao, S., Smith, M. C., Woźniak, P., et al. 2002, MNRAS, 329, 349
Miyamoto, M., & Yoshii, Y. 1995, AJ, 110, 1427
Özel, F., Psaltis, D., Narayan, R., & McClintock, J. E. 2010, ApJ, 725, 1918
Paczynski, B. 1986, ApJ, 304, 1
Paczynski, B. 1991, ApJL, 371, L63
Rowan, D. M., Stanek, K. Z., Jayasinghe, T., et al. 2021, MNRAS, 507, 104
Rybicki, K. A., Wyrzykowski, L., & Klencki, J. 2018, MNRAS, 476, 2013
Sahu, K. C., Anderson, J., Casertano, S., et al. 2017, Sci, 356, 1046
Sahu, K. C., Anderson, J., Casertano, S., et al. 2022, arXiv:2201.13296
Samland, M. 1998, ApJ, 496, 155
Sana, H. 2017, in Proc. of the IAU, IAU Symp. 329, The Lives and Death-Throes of Massive Stars, ed. J. J. Eldridge et al. (Cambridge: Camberidge Univ. Press), 110
Sartore, N., & Treves, A. 2010, A&A, 523, A33
Shapiro, S. L., & Teukolsky, S. A. 1983, Black Holes, White Dwarfs, and Neutron Stars: The Physics of Compact Objects (New York: Wiley)
Skilling, J. 2004, in AIP Conf. Ser., 735, Bayesian Inference and Maximum Entropy Methods in Science and Engineering: 24th Int. Workshop on Bayesian Inference and Maximum Entropy Methods in Science and Engineering, ed. R. Fischer, R. Preuss, & U. V. Toussaint (New York: AIP), 395
Sumi, T. 2008, in Introduction to Microlensing, Manchester Microlensing Conf., 12, ed. M. Kerins et al. (Trieste: SISSA)
Thompson, T. A., Kochanek, C. S., Stanek, K. Z., et al. 2019, Sci, 366, 637
Timmes, F. X., Woosley, S. E., & Weaver, T. A. 1996, ApJ, 457, 834
Udalski, A., Szymanski, M., Kaluzny, J., et al. 1994, AcA, 44, 227
Udalski, A., Szymański, M. K., & Szymański, G. 2015, AcA, 65, 1
Walker, M. A. 1995, ApJ, 453, 37
Wiktorowicz, G., Wyrzykowski, L., & Chruslinska, M. 2019, ApJ, 885, 1
Wyrzykowski, L., Kostrzewa-Rutkowska, Z., Skowron, J., et al. 2016, MNRAS, 458, 3012
Zurlo, A., Gratton, R., Mesa, D., et al. 2018, MNRAS, 480, 236